

# Dynamical explanation for the anomaly in the diffuseness parameter of the nucleus-nucleus potential in heavy-ion fusion reactions

V. Zanganeh,<sup>1,\*</sup> R. Gharaei,<sup>2,†</sup> and N. Wang<sup>3,‡</sup>

<sup>1</sup>*Department of Physics, Sciences Faculty, Golestan University, P. O. Box 49138-15759, Gorgan, Iran*

<sup>2</sup>*Department of Physics, Sciences Faculty, Hakim Sabzevari University, P. O. Box 397, Sabzevar, Iran*

<sup>3</sup>*Department of Physics, Guangxi Normal University, Guilin 541004, People's Republic of China*

(Received 2 January 2017; revised manuscript received 9 February 2017; published 31 March 2017)

The abnormally large diffuseness parameter of the Woods-Saxon (WS) potential in heavy-ion fusion reactions is explained for the first time based on the microscopic dynamics simulations. With the improved quantum molecular dynamic (ImQMD) model, we systematically explore the dynamical processes in the fusion reactions  $^{12}\text{C} + ^{92}\text{Zr}$ ,  $^{16}\text{O} + ^{92}\text{Zr}$ ,  $^{28}\text{Si} + ^{92}\text{Zr}$ ,  $^{35}\text{Cl} + ^{92}\text{Zr}$ ,  $^{40}\text{Ca} + ^{46}\text{Ti}$ , and  $^{16}\text{O} + ^{154}\text{Sm}$ . Without introducing any free model parameters or additional assumptions, the microscopic ImQMD model can reproduce the measured fusion cross sections of all selected colliding systems with good accuracy. Due to the dynamical evolutions of the density distributions in the fusion processes, the energy dependence of nucleus-nucleus potential can be clearly observed. Based on the dynamical nucleus-nucleus potential of the ImQMD simulations, we extract the corresponding diffuseness parameters of the WS potential. The obtained values locate in a range between  $a = 0.83$  and  $1.17$  fm at different incident energies. In addition, the regular decreasing trend for the diffuseness parameter with the increase of the incident energies is also observed.

DOI: [10.1103/PhysRevC.95.034620](https://doi.org/10.1103/PhysRevC.95.034620)

## I. INTRODUCTION

Heavy-ion reaction at energies around the Coulomb barrier is an efficient way to explore the nuclear structures and the synthesis of extremely neutron-deficient nuclei and superheavy elements [1–6]. For light and intermediate heavy systems, the fusion process is usually described by the penetration of the fusion barriers, and the fusion (capture) cross sections can be accurately predicted by using the fusion coupled-channel calculations or empirical barrier distribution approaches [7–11]. The interaction potential between the projectile nuclei and the target nuclei is one of the key quantities in a theoretical description of heavy-ion fusion reactions. For head-on collisions, the potential is usually defined as the sum of two parts: the long-range Coulomb repulsion and the short-range nuclear attraction. The Coulomb part of the interaction potential can be described well especially before the neck is formed, whereas the nuclear part is still not well constrained. The accurate description of the nuclear potential for heavy-ion fusion and scattering is a challenging task in nuclear physics.

To describe the nucleus-nucleus potential, a large number of empirical nuclear potential were proposed in recent decades [12–15]. In these nuclear potentials, the Woods-Saxon (WS) form

$$V_{\text{ws}}(r) = \frac{V_0}{1 + \exp[(r - R_0)/a]} \quad (1)$$

is a widely used form, with the depth of the potential  $V_0$ , the radius  $R_0 = r_0(A_1^{1/3} + A_2^{1/3})$ , and the diffuseness parameter  $a$ .

In the WS parametrization of nuclear potential, the diffuseness parameter is one of the key parameters which affects the slope of the nuclear potential in the surface region and thus the curvature of the Coulomb barrier. From the elastic scattering data, one extracted the diffuseness parameter with a value of  $a = 0.63$  fm [16–18], whereas it is shown that a larger value is required for reproducing the experimental fusion data, e.g.,  $a = 0.75$  to  $1.5$  fm [19–27]. In recent years, the surface diffuseness anomaly has attracted much attention in heavy-ion fusion and scattering research field. For example, Ghodsi and Zanganeh employed the M3Y-type nucleon-nucleon forces with additional repulsive interactions to calculate the interaction potential in the fusion reactions [28]. They found that the correction effects of these repulsion interactions leads to an increased value of  $0.73$  fm for the diffuseness parameter. In other words, it is suggested that the incompressibility of the cold nuclear matter could be responsible for the unexpected behavior of the diffuseness parameter in the fusion process. In another systematic study, M. Singh *et al.* [29] proposed an energy-dependent form for the diffuseness parameter of WS potential which are phenomenologically parameterized at the energies around the fusion barrier. Their theoretical predictions are in good agreement with experimental data of the fusion excitation functions in the different projectile and target combinations using the parameterized form of  $a(E)$  supplemented with the coupled-channel effects. The authors demonstrated that the diffuseness parameter has a decreasing trend with incident energy, (e.g., for  $^{32,36}\text{S} + ^{90}\text{Zr}$  the diffuseness parameter decreases from  $a = 0.97$  fm at an incident energy of  $E_{\text{c.m.}} = 70$  MeV to  $0.85$  fm at  $100$  MeV). In addition, Chushnyakova and Gontchar [30] applied the classical dissipative trajectory model and varied the diffuseness of the charge density in the double-folding potential as the consequence of dynamical effects to explain the abnormally large diffuseness of the nucleus-nucleus potential. They concluded that the

\*v.zanganeh@gu.ac.ir

†r.gharaei@hsu.ac.ir

‡wangning@gxnu.edu.cn

anomaly of diffuseness parameter is not in the potential itself but in the dynamical character of the colliding process.

The microscopic dynamics transport models could be helpful for understanding of the anomaly of diffuseness parameter, since the whole fusion process of a reaction system, e.g., the time evolution of density distributions of the system, can be described self-consistently, without introducing additional assumptions. During the fusion process, the dynamic effects, such as the dynamical deformation effects of the reaction partners, the energy dependence of the nuclear densities, the nucleon transfer, and the effects of the cold nuclear matter play an important role, especially in the overlapping region of the interacting nuclei [31–36]. It is expected that these dynamical effects strongly influence the surface diffuseness of the interacting nuclei at the touching configurations. It is therefore interesting to investigate the behavior of nuclear surface in the fusion process with a microscopic dynamics model. In recent years, various dynamical approaches such as TCSM and TDHF models have been used for calculating the internuclear potential in the fusion process [37–40]. Another semiclassical approach to analyze the fusion reactions for heavy ions has been proposed in the literature [41]. The authors incorporated quantal zero-point fluctuations of the surface vibrations in a stochastic approximation. This stochastic semiclassical model has been employed to calculate fusion cross sections of Ni isotopes.

In this work, we attempt to explore the physics behind the anomaly of diffuseness parameter by using the improved quantum molecular dynamic (ImQMD) model for systematically simulating the fusion processes. As an extended version of the quantum molecular dynamics (QMD) model, the ImQMD model was proposed for the study of heavy-ion reactions at energies around the Coulomb barrier, in which the standard Skyrme force is adopted for describing not only the bulk properties but also the surface properties of nuclei, and the Fermi constraint is used to simulate the effects of antisymmetrization and to improve the stability of an individual nucleus and fragments. In addition to successfully describing heavy-ion fusion reactions at energies around the Coulomb barrier [42–47], the ImQMD model was also successfully applied to multifragmentation and multinucleon transfer reactions [48,49]. From the point of view of the semiclassical ImQMD model based on event-by-event simulations, the sub-barrier fusion is a process that the rare projectile nuclei surmount rather than tunnel through the suppressed potential barrier.

The structure of this paper is as follows: In Sec. II, the framework of the ImQMD model is briefly introduced. In Sec. III, the time evolution of the nuclear density distributions at different energies are investigated. In addition, the calculated interaction potential and the fusion excitation functions are also presented. Finally, the conclusions are drawn in Sec. IV.

## II. FRAMEWORK OF THE ImQMD MODEL

In the ImQMD model, the density distribution function  $\rho$  of a system reads

$$\rho(\mathbf{r}) = \sum_i \frac{1}{(2\pi\sigma_r^2)^{3/2}} \exp\left[-\frac{(\mathbf{r}-\mathbf{r}_i)^2}{2\sigma_r^2}\right], \quad (2)$$

where  $\sigma_r$  represents the spatial spread of the wave packet. In fact, each nucleon is represented by a coherent state of a Gaussian wave packet. The propagation of nucleons is governed by Hamiltonian equations of motion under the self-consistently generated mean field,

$$\dot{\mathbf{r}}_i = \frac{\partial H}{\partial \mathbf{p}_i}, \quad \dot{\mathbf{p}}_i = -\frac{\partial H}{\partial \mathbf{r}_i}, \quad (3)$$

where  $r_i$  and  $p_i$  are the center of the  $i$ th wave packet in the coordinate and momentum space, respectively. The initial condition is very important in QMD calculations. In the present work, the preparation of initial nuclei is completely investigated in Refs. [42,43,45]. The Hamiltonian  $H$  consists of the kinetic energy  $T = \sum_i \frac{p_i^2}{2m}$ , the nuclear interaction potential energy, and the Coulomb interaction potential energy,

$$H = T + U_{\text{loc}} + U_{\text{Coul}}, \quad (4)$$

where  $U_{\text{loc}} = \int V_{\text{loc}}(\mathbf{r})d\mathbf{r}$  is obtained from the standard Skyrme energy density functional,

$$V_{\text{loc}} = \frac{\alpha}{2} \frac{\rho^2}{\rho_0} + \frac{\beta}{\gamma+1} \frac{\rho^{\gamma+1}}{\rho_0^\gamma} + \frac{g_{\text{sur}}}{2\rho_0} (\nabla\rho)^2 + g_\tau \frac{\rho^{\eta+1}}{\rho_0^\eta} + \frac{C_s}{2\rho_0} [\rho^2 - k_s (\nabla\rho)^2] \delta^2 \quad (5)$$

with isospin asymmetry  $\delta = (\rho_n - \rho_p)/(\rho_n + \rho_p)$ .  $U_{\text{Coul}}$  is the Coulomb interaction potential energy which includes the contribution of the direct and exchange terms, with the latter being taken into account in the Slater approximation.

To describe the fermionic nature of the  $N$ -body system and to improve the stability of an individual nucleus the modified Fermi constraint is adopted. In the Fermi constraint which was previously proposed by Papa *et al.* in the CoMD model [50] and improved very recently in Refs. [48,51], the phase space occupation probability  $\tilde{f}_i$  of the  $i$ th particle is checked during the propagation of nucleons. If  $\tilde{f}_i > 1$ , i.e., violation of the Pauli principle, the momentum of the particle  $i$  is randomly changed by a series of two-body elastic scattering and inelastic scattering between this particle and its neighboring particles, together with Pauli blocking condition being checked after the momentum redistribution. In other words, both the self-consistently generated mean field and the momentum redistribution in the Fermi constraint which introduces additional fluctuations and two-body dissipation affect the movements of nucleons in the simulations. In this work, we adopt the parameter set IQ3 [47].

## III. RESULTS AND DISCUSSIONS

To understand the influence of the dynamical process on the interaction potential between the reaction partners, we study the time evolution of the nuclear density distributions of the projectile and target nuclei. In the present work, we focus on the fusion reactions  $^{12}\text{C} + ^{92}\text{Zr}$ ,  $^{16}\text{O} + ^{92}\text{Zr}$ ,  $^{28}\text{Si} + ^{92}\text{Zr}$ ,  $^{35}\text{Cl} + ^{92}\text{Zr}$ ,  $^{40}\text{Ca} + ^{46}\text{Ti}$ , and  $^{16}\text{O} + ^{154}\text{Sm}$ .

In Fig. 1, we show the time evolution of the density distributions of the projectile-like and the target-like in the fusion reaction  $^{40}\text{Ca} + ^{46}\text{Ti}$  with the impact parameter  $b = 0$  fm at two different incident energies  $E_{\text{c.m.}} = 65$  MeV

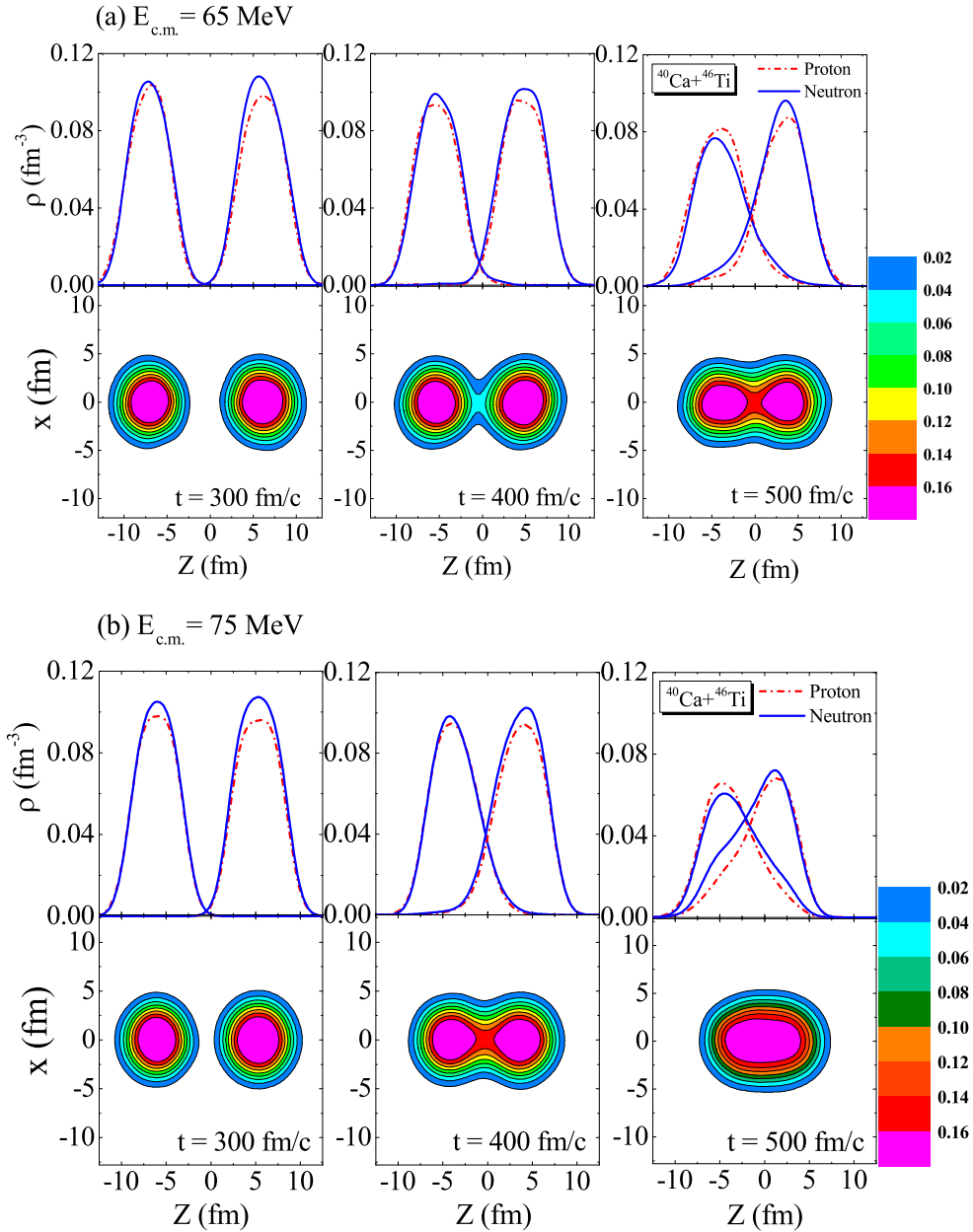


FIG. 1. Time evolution of density distribution for head-on collisions of  $^{40}\text{Ca} + ^{46}\text{Ti}$  at two incident energies: (a)  $E_{c.m.} = 65$  MeV and (b)  $E_{c.m.} = 75$  MeV.

and  $E_{c.m.} = 75$  MeV. Here, the density distribution is averaged on the fusion events for the head-on collision with the parameter set IQ3. For this reaction, the most probable barrier height is 58.4 MeV, according to the barrier distribution function in the extended Thomas-Fermi approach together with the Skyrme energy density functional [52]. Here, we show the density distributions of the reaction system at  $t = 300, 400,$  and  $500$  fm/c. One can see that the dynamical effects strongly influence the surface region of the nuclear densities at the neck side. One should note that the saturation property of the cold nuclear matter and nucleon transfer play an important role in the fusion process, whereas the situation is quite different in the static approach; see, for example, Fig. 1 of Ref. [53].

Comparing the density distributions of the interacting nuclei at the same time but different incident energies, one sees that the neck evolution and nuclear surface diffuseness at the neck side are energy dependent. It is attributed to the increase of the nucleon exchange between the reaction partners with incident energy at head-on collisions.

It is expected that the change of the nuclear density distributions during the fusion process affects the total interaction potential between the projectile and target nuclei. To understand the influence of the dynamical effects on the nuclear potential, we show the calculated interaction potential in Fig. 2 for two fusion reactions  $^{16}\text{O} + ^{92}\text{Zr}$  and  $^{28}\text{Si} + ^{92}\text{Zr}$  at different incident energies as a function of the center-to-center

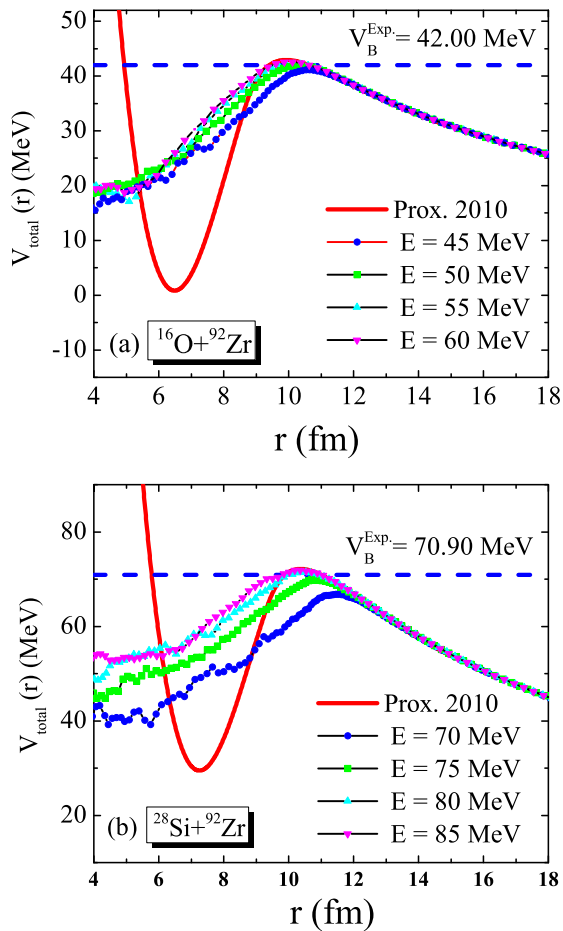


FIG. 2. Dynamical nucleus-nucleus potentials for the fusion reactions  $^{16}\text{O} + ^{92}\text{Zr}$  and  $^{28}\text{Si} + ^{92}\text{Zr}$  at different incident energies  $E_{c.m.}$ . Solid curve denotes the static proximity potential [15].

distance  $r$  (in fm) by using the ImQMD model. We create 500 reaction events for head-on collision which for each event, we evolve the reaction system for a time of 1000 fm/c. Moreover, the distance between the projectile and the target at the initial time is set to 40 fm for these reactions. The static nucleus-nucleus potential from the proximity potential [15] are also presented for comparison. One should note that with increasing of the incident energy, the nucleons in the individual nuclei have not enough time to readjust the density distributions for lowering the barrier height before the neck is well formed. In other words, it is expected that the barrier height of the dynamical nucleus-nucleus potential approaches to the result under the frozen density approximation at the incident energies much higher than the Coulomb barrier.

From Fig. 2, we find that the dynamical barrier height increases with increase of the bombarding energy of the projectile and gradually reaches the static one. As pointed before, the fully microscopic density-constrained TDHF is utilized as a novel approach for calculating the ion-ion potential [38,39,54,55] which can incorporate all of the dynamical effects such as neck formation, particle exchange, internal excitations, and deformation effects into potential [56]. This model predicts an energy-dependent behavior for interacting

potential in different fusion reactions, including heavy systems such as  $^{132}\text{Sn} + ^{40,48}\text{Ca}$  [55] and even in reaction between a light and heavy nucleus such as  $^{16}\text{O} + ^{208}\text{Pb}$  [57]. An important conclusion drawn from those studies is that the height of the fusion barrier increase by increasing the collision energy. We also note the capture pocket in the Proximity potential model [15] is deeper than those obtained from the ImQMD model.

With the ImQMD model, the fusion cross sections can be calculated by generating a large number of simulation events (about 100) at each incident energy  $E_{c.m.}$  and at each impact parameter  $b$ , and counting the number of fusion ones. We obtain the probability of fusion reaction  $g_{\text{fus}}(E_{c.m.}, b)$ , by which the fusion cross section can be calculated [42]

$$\sigma_{\text{fus}}(E_{c.m.}) = 2\pi \int b g_{\text{fus}} db \simeq 2\pi \sum b g_{\text{fus}} \Delta b. \quad (6)$$

The initial distance between the projectile and target is taken to be  $R = 40$  fm for calculating the fusion cross sections. It is therefore necessary to check the reliability of the model for the description of the dynamical potential and fusion cross section, based on the measured fusion excitation functions. The obtained fusion excitation functions for  $^{12}\text{C} + ^{92}\text{Zr}$ ,  $^{16}\text{O} + ^{92}\text{Zr}$ ,  $^{28}\text{Si} + ^{92}\text{Zr}$ ,  $^{35}\text{Cl} + ^{92}\text{Zr}$ ,  $^{40}\text{Ca} + ^{46}\text{Ti}$ , and  $^{16}\text{O} + ^{154}\text{Sm}$  colliding systems are shown in Fig. 3. One can see that the fusion data can be reproduced reasonably well with the ImQMD simulations, especially at energies slightly lower than the fusion barrier. As a result of the literature, we can also explain the measured fusion cross sections at below and above Coulomb barrier energies for different fusion reactions using the other microscopic approaches such as the DC-TDHF model—see, for example, Refs. [54,55,57]—whereas, the theoretical results of the previous studies such as those in Refs. [28,53] indicate that the standard static approaches underestimate these data at sub-barrier energies.

Based on the dynamical interaction potential from the ImQMD model, we extract the corresponding diffuseness parameter  $a$  in the Woods-Saxon potential. Here, the values of this parameter are determined by fitting the dynamical potentials with a Woods-Saxon form and varying the parameter  $a$  around the fusion barrier radii. For each considered fusion reaction, one can show that the extracted diffuseness parameters are not very sensitive upon the choice of the depth and the radius parameters. Therefore, the values of these parameters are considered fixed to extract the diffuseness parameter of the WS potential at different incident energies. Figure 4 shows the trend of the diffuseness parameter  $a$  versus the center-of-mass energy  $E_{c.m.}$  for all of the selected fusion reactions [19,58,59]. The constant value of  $a = 0.63$  fm extracted from the scattering data is also given in Fig. 4 by the horizontal dashed lines. We find that the obtained diffuseness parameter from the ImQMD with the values locate in the range of 0.83 to 1.17 fm is systematically larger than 0.63 fm. In addition, we note that the extracted values of the diffuseness parameter have a regular decreasing trend with the increase of incident energy. As mentioned previously, the energy dependence of the diffuseness parameter  $a$  has also been examined by Singh *et al.* [29]. For  $^{12}\text{C} + ^{92}\text{Zr}$  and  $^{28}\text{Si} + ^{92}\text{Zr}$ , as an example, we also show the results of Singh

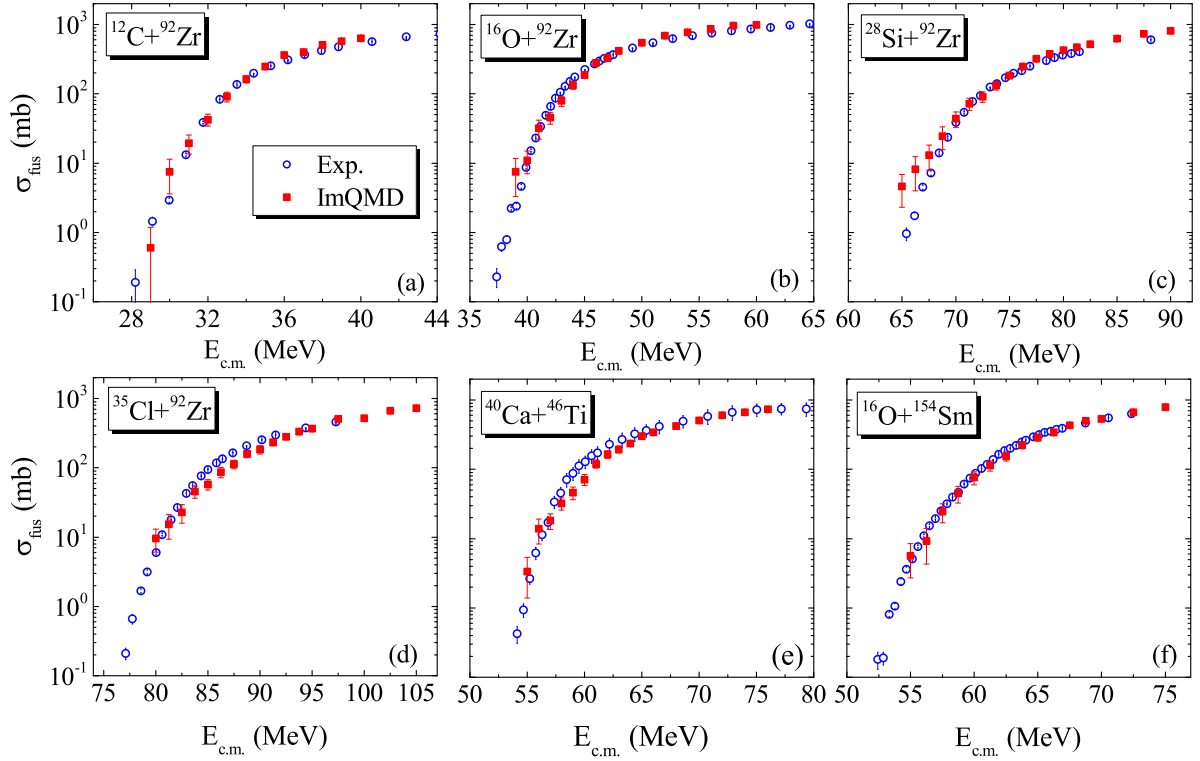


FIG. 3. Fusion excitation functions for the fusion reactions (a)  $^{12}\text{C} + ^{92}\text{Zr}$ , (b)  $^{16}\text{O} + ^{92}\text{Zr}$ , (c)  $^{28}\text{Si} + ^{92}\text{Zr}$ , (d)  $^{35}\text{Cl} + ^{92}\text{Zr}$ , (e)  $^{40}\text{Ca} + ^{46}\text{Ti}$ , and (f)  $^{16}\text{O} + ^{154}\text{Sm}$ . The open and solid circles denote the experimental data and the results of the ImQMD model, respectively. The experimental data are taken from Refs. [19,58,59].

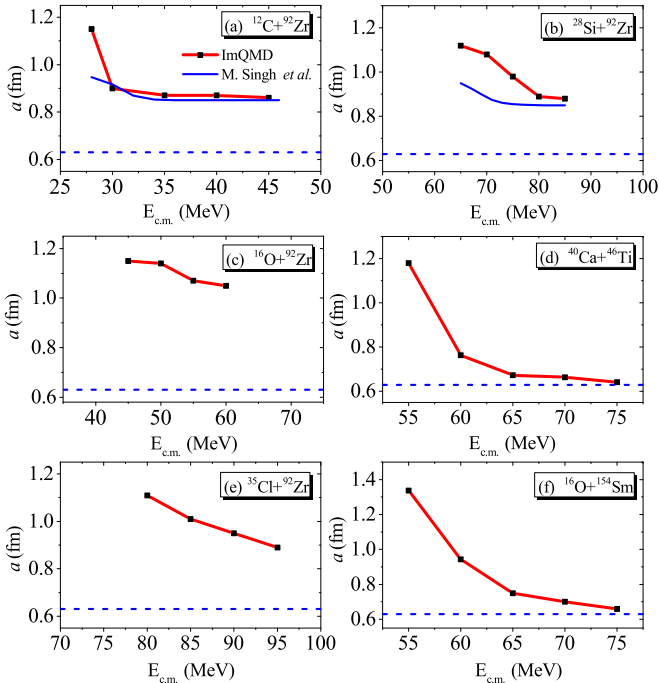


FIG. 4. Extracted diffuseness parameter as a function of incident energy. In panels (a) and (b), the solid curves denote the results of M. Singh *et al.* [29], for example. The estimation error of fitting the WS potential to the dynamical potentials is less than  $10^{-7}$ .

*et al.* in Fig. 4 (solid curves) for comparison. We find that both models give a similar decreasing trend for the energy dependence of the diffuseness parameter.

#### IV. CONCLUSIONS

In this work, we have investigated six heavy-ion fusion reactions with a microscopic dynamics model. The interaction potentials and fusion cross sections of for  $^{12}\text{C} + ^{92}\text{Zr}$ ,  $^{16}\text{O} + ^{92}\text{Zr}$ ,  $^{28}\text{Si} + ^{92}\text{Zr}$ ,  $^{35}\text{Cl} + ^{92}\text{Zr}$ ,  $^{40}\text{Ca} + ^{46}\text{Ti}$ , and  $^{16}\text{O} + ^{154}\text{Sm}$  are systematically studied by using the improved quantum molecular dynamics (ImQMD) model under the parameter set IQ3. We find the following results:

- (1) In the time evolution of a fusion system, the dynamical effects such as nucleon transfer and dynamical deformation strongly influence the density distributions of the reaction partners, especially the surface region at neck side when the projectile nuclei approaching the target.
- (2) The dynamical effects lead to a distribution of the fusion barriers due to the fluctuations and dissipations, instead of a single barrier from the static approach.
- (3) The energy dependence of the interaction potential can be clearly observed and the measured fusion cross sections for these reactions can be well reproduced by using the ImQMD model, without introducing any additional parameters or assumptions.

- (4) The diffuseness parameter represented in the Woods-Saxon potential has a regular decreasing trend with the incident energy at energies around the Coulomb barrier.
- (5) The dynamical effects play a key role to the surface diffuseness anomaly in the heavy-ion fusion reactions.

## ACKNOWLEDGMENTS

This work was supported by National Natural Science Foundation of China (Grants No. 11275052, No. 11422548, and No. 11547307) and Guangxi Natural Science Foundation (No. 2015GXNSFDA139004).

- 
- [1] M. Dasgupta, D. J. Hinde, A. Diaz-Torres, B. Bouriquet, C. I. Low, G. J. Milburn, and J. O. Newton, *Phys. Rev. Lett.* **99**, 192701 (2007).
- [2] S. A. Kalandarov, G. G. Adamian, N. V. Antonenko, and J. P. Wieleczko, *Phys. Rev. C* **93**, 054607 (2016).
- [3] H. Q. Zhang, C. J. Lin, F. Yang, H. M. Jia *et al.*, *Phys. Rev. C* **82**, 054609 (2010).
- [4] Y. T. Oganessian *et al.*, *Phys. Rev. Lett.* **104**, 142502 (2010).
- [5] A. Sobczewski and K. Pomorski, *Prog. Part. Nucl. Phys.* **58**, 292 (2007).
- [6] R. K. Gupta, M. Manhas, G. Muenzenberg, and W. Greiner, *Phys. Rev. C* **72**, 014607 (2005).
- [7] C. Y. Wong, *Rev. Lett.* **31**, 766 (1973).
- [8] K. Hagino, N. Rowley, and A. T. Kruppa, *Comput. Phys. Commun.* **123**, 143 (1999).
- [9] N. Wang, M. Liu, and Y. X. Yang, *Sci. China Ser. G* **52**, 1554 (2009).
- [10] R. K. Puri and R. K. Gupta, *Phys. Rev. C* **45**, 1837 (1992).
- [11] B. Wang, K. Wen, W. J. Zhao, E. G. Zhao, and S. G. Zhou, *At. Data Nucl. Data Tables* **114**, 281 (2017).
- [12] R. Bass, *Deep-Inelastic and Fusion Reactions with Heavy Ions*, Lecture Notes in Physics, Vol. 117 (Spring, Berlin, 1980), pp. 281–293.
- [13] R. A. Broglia and A. Winther, *Heavy Ion Reactions*, in Frontiers in Physics Lecture Note Series, Vol. 84 (Addison-Wesley, Redwood City, CA, 1991).
- [14] C. K. Phookan and K. Kalita, *Nucl. Phys. A* **899**, 29 (2013).
- [15] I. Dutt and R. K. Puri, *Phys. Rev. C* **81**, 064609 (2010).
- [16] P. R. Christensen and A. Winther, *Phys. Lett. B* **65**, 19 (1976).
- [17] L. C. Chamon, L. C. Chamon, D. Pereira Jr., E. S. Rossi, C. P. Silva, H. Dias, L. Losano, and C. A. P. Ceneviva, *Nucl. Phys. A* **597**, 253 (1996).
- [18] C. P. Silva, M. A. G. Alvarez, L. C. Chamon *et al.*, *Nucl. Phys. A* **679**, 287 (2001).
- [19] J. O. Newton, C. R. Morton, M. Dasgupta, J. R. Leigh, J. C. Mein, D. J. Hinde, H. Timmers, and K. Hagino, *Phys. Rev. C* **64**, 064608 (2001).
- [20] I. I. Gontchar, D. J. Hinde, M. Dasgupta, and J. O. Newton, *Nucl. Phys. A* **722**, C479 (2003).
- [21] J. O. Newton, R. D. Butt, M. Dasgupta, D. J. Hinde, I. I. Gontchar, C. R. Morton, and K. Hagino, *Phys. Rev. C* **70**, 024605 (2004).
- [22] A. Mukherjee, D. J. Hinde, M. Dasgupta, K. Hagino, J. O. Newton, and R. D. Butt, *Phys. Rev. C* **75**, 044608 (2007).
- [23] K. Hagino, T. Takehi, A. B. Balantekin, and N. Takigawa, *Phys. Rev. C* **71**, 044612 (2005).
- [24] J. O. Newton, R. D. Butt, M. Dasgupta, D. J. Hinde, I. I. Gontchar, C. R. Morton, and K. Hagino, *Phys. Lett. B* **586**, 219 (2004).
- [25] K. Hagino, N. Rowley, and M. Dasgupta, *Phys. Rev. C* **67**, 054603 (2003).
- [26] G. Montagnoli, A. M. Stefanini, L. Corradi, S. Courtin, E. Fioretto, F. Haas, D. Lehbertz, F. Scarlassara, R. Silvestri, and S. Szilner, *Phys. Rev. C* **82**, 064609 (2010).
- [27] V. V. Sargsyan, G. G. Adamian, N. V. Antonenko, and R. P. S. Gomes, *Eur. Phys. J. A* **50**, 184 (2014).
- [28] O. N. Ghodsi and V. Zanganeh, *Nucl. Phys. A* **846**, 40 (2010).
- [29] M. Singh, S. S. Duhan, and R. Kharab, *Mod. Phys. Lett. A* **26**, 2129 (2011).
- [30] M. V. Chushnyakova and I. I. Gontchar, *Phys. Rev. C* **87**, 014614 (2013).
- [31] M. Beckerman, M. Salomaa, A. Sperduto, J. D. Molitoris, and A. DiRienzo, *Phys. Rev. C* **25**, 837 (1982).
- [32] N. Wang, X. Wu, and Z. Li, *Chin. Phys. Lett.* **20**, 1466 (2003).
- [33] N. Wang, X. Wu, and Z. Li, *Phys. Rev. C* **67**, 024604 (2003).
- [34] C. L. Jiang, B. B. Back, H. Esbensen, R. V. F. Janssens, and K. E. Rehm, *Phys. Rev. C* **73**, 014613 (2006).
- [35] C. L. Jiang *et al.*, *Phys. Rev. C* **71**, 044613 (2005).
- [36] S. Misiu and H. Esbensen, *Phys. Rev. Lett.* **96**, 112701 (2006).
- [37] R. K. Gupta, R. Aroumougame, and N. Malhotra, *Lett. Nuovo Cimento* **32**, 137 (1981).
- [38] A. S. Umar and V. E. Oberacker, *Phys. Rev. C* **74**, 021601(R) (2006).
- [39] A. S. Umar and V. E. Oberacker, *Phys. Rev. C* **76**, 014614 (2007).
- [40] K. Washiyama and D. Lacroix, *Phys. Rev. C* **78**, 024610 (2008).
- [41] S. Ayik, B. Yilmaz, and D. Lacroix, *Phys. Rev. C* **81**, 034605 (2010).
- [42] N. Wang, Z. Li, and X. Wu, *Phys. Rev. C* **65**, 064608 (2002).
- [43] N. Wang, Z. Li, X. Wu, J. Tian, Y. X. Zhang, and M. Liu, *Phys. Rev. C* **69**, 034608 (2004).
- [44] Y. Zhang and Z. Li, *Phys. Rev. C* **74**, 014602 (2006).
- [45] N. Wang, L. Ou, Y. Zhang, and Z. Li, *Phys. Rev. C* **89**, 064601 (2014).
- [46] Y. Jiang, N. Wang, Z. Li, and W. Scheid, *Phys. Rev. C* **81**, 044602 (2010).
- [47] V. Zanganeh, N. Wang, and O. N. Ghodsi, *Phys. Rev. C* **85**, 034601 (2012).
- [48] N. Wang, T. Wu, J. Zeng, Y. X. Yang, and L. Ou, *J. Phys. G: Nucl. Part. Phys.* **43**, 065101 (2016).
- [49] N. Wang and L. Guo, *Phys. Lett. B* **760**, 236 (2016).
- [50] M. Papa, T. Maruyama, and A. Bonasera, *Phys. Rev. C* **64**, 024612 (2001).
- [51] N. Wang, K. Zhao, and Z. X. Li, *Sci. China-Phys. Mech. Astron.* **58**, 112001 (2015).
- [52] M. Liu, N. Wang *et al.*, *Nucl. Phys. A* **768**, 80 (2006).
- [53] O. N. Ghodsi and R. Gharai, *Phys. Rev. C* **84**, 024612 (2011).
- [54] A. S. Umar, C. Simenel, and V. E. Oberacker, *Phys. Rev. C* **89**, 034611 (2014).

- [55] V. E. Oberacker and A. S. Umar, *Phys. Rev. C* **87**, 034611 (2013).
- [56] A. S. Umar and V. E. Oberacker, *Phys. Rev. C* **77**, 064605 (2008).
- [57] A. S. Umar and V. E. Oberacker, *Eur. Phys. J. A* **39**, 243 (2009).
- [58] A. A. Sonzogni, J. D. Bierman, M. P. Kelly, J. P. Lestone, J. F. Liang, and R. Vandenbosch, *Phys. Rev. C* **57**, 722 (1998).
- [59] J. R. Leigh, M. Dasgupta, D. J. Hinde, J. C. Mein, C. R. Morton, R. C. Lemmon, J. P. Lestone, J. O. Newton, H. Timmers, J. X. Wei, and N. Rowley, *Phys. Rev. C* **52**, 3151 (1995).